Article:
De Pablos, Luis M, Ferreira, Tiago R, Dowle, Adam et al. (4 more authors) (2019) The mRNA-bound proteome of Leishmania mexicana : novel genetic insight into an ancient parasite. Molecular and Cellular Proteomics. pp. 1271-1284. ISSN 1535-9476

https://doi.org/10.1074/mcp.RA118.001307

The mRNA-bound Proteome of *Leishmania mexicana*: Novel Genetic Insight into an Ancient Parasite

Authors

Luis M. de Pablos, Tiago R. Ferreira, Adam A. Dowle, Sarah Forrester, Ewan Parry, Katherine Newling, and Pegine B. Walrad

Correspondence

pegine.walrad@york.ac.uk

Graphical Abstract

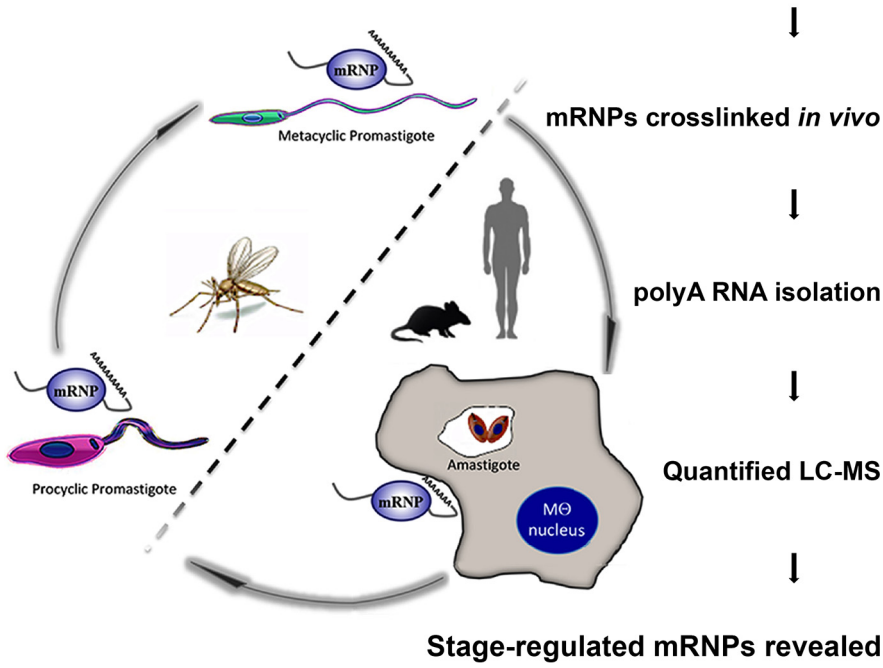

In Brief

A comprehensive, quantified identification of the mRNA-binding and whole cell proteomes in the three main *Leishmania* lifecycle stages, the first such comparison in kinetoplastid parasites, demonstrates *trans*-regulator RBPs select distinct, specific mRNA target pools in a stage-regulated manner despite equivalent, constitutive transcript levels available. Results further indicate that in *L. mexicana* parasites, mRNA levels are not a strong predictor of whole cell expression or RNA binding potential of encoded proteins. Included are the first proteomes from the human-infective metacyclic promastigote stage.

Highlights

- Comprehensive, quantified mRNA-binding and whole cell proteomes of the three main *Leishmania* spp. lifecycle stages.
- Decisive evidence that *trans*-regulator RBPs can selectively bind distinct mRNA target pools in a stage-regulated manner despite equivalent transcript levels.
- Quantified evidence that in *L. mexicana* parasites, mRNA levels are not a strong predictor of whole cell expression or RNA binding potential of encoded proteins.
- Use of *Histone H4* as the first marker of procyclic stage cells in *Leishmania* spp.

de Pablos et al., 2019, Molecular & Cellular Proteomics *18*, 1271–1284

https://doi.org/10.1074/mcp.RA118.001307

⌘ *Author's Choice*

The mRNA-bound Proteome of *Leishmania mexicana*: Novel Genetic Insight into an Ancient Parasite*

Luis M. de Pablos‡‡‡‖, Tiago R. Ferreira‡‡‡**, Adam A. Dowle§, Sarah Forrester‡, Ewan Parry‡, Katherine Newling¶, and Pegine B. Walrad‡§§

Leishmania **parasite infections, termed the leishmaniases, cause significant global infectious disease burden. The lifecycle of the parasite embodies three main stages that require precise coordination of gene regulation to survive environmental shifts between sandfly and mammalian hosts. Constitutive transcription in kinetoplastid parasites means that gene regulation is overwhelmingly reliant on post-transcriptional mechanisms, yet strikingly few *Leishmania trans*-regulators are known. Using optimized crosslinking and deep, quantified mass spectrometry, we present a comprehensive analysis of 1400 mRNA binding proteins (mRBPs) and whole cell proteomes from the three main *Leishmania* lifecycle stages. Supporting the validity, although the crosslinked RBPome is magnitudes more enriched, the protein identities of the crosslinked and non-crosslinked RBPomes were nearly identical. Moreover, multiple candidate RBPs were endogenously tagged and found to associate with discrete mRNA target pools in a stage-specific manner. Results indicate that in *L. mexicana* parasites, mRNA levels are not a strong predictor of the whole cell expression or RNA binding potential of encoded proteins. Evidence includes a low correlation between transcript and corresponding protein expression and stage-specific variation in protein expression *versus* RNA binding potential. Unsurprisingly, RNA binding protein enrichment correlates strongly with relative replication efficiency of the specific lifecycle stage. Our study is the first to quantitatively define and compare the mRBPome of multiple stages in kinetoplastid parasites. It provides novel, in-depth insight into the *trans*-regulatory mRNA:Protein (mRNP) complexes that drive *Leishmania* parasite lifecycle progression.** ***Molecular & Cellular Proteomics 18: 1271–1284, 2019. DOI: 10.1074/mcp.RA118.001307.***

Leishmania spp. parasites are the causative agent of leishmaniasis, a neglected disease that represents the ninth largest global infectious disease burden (1). These protozoa have a dixenous lifecycle that transitions between multiple promastigote stages in the sandfly vector to the amastigote stage in the phagolysosomes of mammalian immune cells (2). Distinct environmental conditions (pH, temperature, nutrient availability) serve as triggers for developmental events. For parasite lifecycle progression, both metacyclogenesis (procyclic to metacyclic promastigote) and amastigogenesis (metacyclic promastigote to amastigote) differentiation processes require tightly coordinated gene regulation (2). To date, many *cis*-elements but strikingly few *trans*-regulators have been implicated in *Leishmania* developmental progression (3–11). The identification of *Leishmania trans*-regulators that bind mRNAs in a stage-specific manner lends vital insight into the cellular processes which promote and enable parasite survival.

Regulation of gene expression requires fine-tuned, coordinated mechanisms that respond to shifting environmental conditions. Kinetoplastid parasites rely almost exclusively on post-transcriptional gene regulatory mechanisms because of their constitutive transcription of Pol II-driven polycistronic gene arrays (2). Accordingly, RNA binding proteins (RBPs)[1] are overrepresented in the proteome of these organisms in line with their role as the primary gene regulators. Such *trans*-regulatory RBPs dynamically bind to mRNA forming ribonucleoprotein complexes (mRNPs) that regulate the trafficking and processing of mRNA molecules from synthesis to decay (12). Environmental pressures stimulate swift changes in mRNP localization, composition and function that accelerate rates of mRNA translation, decay, or sequestration to intracellular granules in response (13).

Previous large-scale isolations of mRNA-bound proteomes have identified candidate regulators in yeast, flies, mice, and humans (14, 15). More recently, kinetoplastid parasite mRNP investigations yielded 155 RBPs in *Trypanosoma brucei* monomorphic bloodstream forms and 128 *Leishmania donovani* RBPs in axenic amastigote forms (16, 17). These studies

From the ‡Centre for Immunology and Infection, §Metabolomics and Proteomics Lab, Bioscience Technology Facility, and ¶Genomics and Bioinformatics Lab, Bioscience Technology Facility, Department of Biology, University of York, UK

Received December 29, 2018, and in revised form, February 23, 2019
Published, MCP Papers in Press, April 4, 2019, DOI 10.1074/mcp.RA118.001307

were refined in scope to only one lifecycle stage, yet importantly confirm that mRNA-bound factors in kinetoplastid cells include proteins without canonical RNA-binding motifs (14–18).

Here we present the mRNA-bound as well as whole cell proteomes isolated from *L. mexicana* procyclic promastigote ("PCF"), metacyclic promastigote ("META"), and amastigote ("AMA") stage parasites. We have identified over 1400 mRNA bound proteins (RBPs) represented by at least two unique peptides in both UV-crosslinked (XL) and non-crosslinked (nonXL) samples, the XL samples being magnitudes higher in overall enrichment because of the covalent bonds strengthening interactions. The isolated mRNA-bound proteomes are differentially enriched and over 250 RBPs exhibit stage-specific expression. In addition, the whole cell proteomes of these stages were also quantitatively identified in triplicate for comparative use in this study and represent an essential resource for the *Leishmania* and eukaryotic research community. Of 8144 predicted proteins, our analysis identified over 2400 with at least 2 high quality unique peptides, of which nearly half fluctuate in expression levels throughout the lifecycle. Of interest, bioinformatics and biochemical analyses indicate only a minority of identified proteins display expression patterns like their encoding transcripts. Further, the expression of an mRNA binding protein does not correlate to RNA association. Importantly, these findings may implicate post-translational modifications in the fluctuations of RNA binding potential and relative stability of candidate *trans*-regulators as well as overall cellular translational capacity and activity.

EXPERIMENTAL PROCEDURES

Parasite Culture and Purification—Early passage (P2-P3) PCF forms of *L. mexicana* strain M379 (MNYC/BZ/62/M379) were isolated from log phase (3–6e^6 cells/ml) in M199 medium (pH 7.2) at 26 °C (19). META-enriched cultures were generated as previously described (20). Briefly, PCF forms innoculated Grace's media (10% hiFCS, 1% Pen/Strep, 1X BME vitamins, pH 5.5) at 1.5 × 10^5 cells/ml and cultured for 7 days at 26 °C. For J774.2 macrophage (MØ; (Sigma)) infection assays, META-enriched cultures were isolated via resistance to complement-mediated lysis in 20% human serum (Sigma) for 30min at 37 °C and validated via *sherp* expression (21, 22).

Validated META parasites were centrifuged and resuspended in complete DMEM medium (10% hiFCS, 1% Penicillin/Streptomycin, 2 mM L-glutamine) and used to infect J774.2 MØ cultures at a 15:1 parasite/MØ ratio (1.25 × 10^7 MØ/plate) for 6 h at 34 °C before washing 3× with prewarmed PBS, incubation in DMEM medium at 34 °C for 18 h, UV irradiation (or not), disruption of MØs and isolation of 24 h post-infection (pi) intracellular amastigote forms (AMA(MØ)) using either a 45% Percoll or sucrose gradient as described (6).

Mouse Infections—To isolate AMA(LD) parasites *in vivo*, 1 × 10^7 serum-treated META *L. mexicana* cells were injected in rumps of 8–12 week old Balb/c mice (Charles River, UK). After 4 months the mice were sacrificed and the lesions harvested as described (6, 23). For ethical reasons, AMA(LD) were harvested only for XL mRNP samples.

Isolation of Leishmania mRNA-bound Proteomes—For the mRNA interactome capture experiments, all conditions were equivalent for the *Leishmania* lifecycle forms PCF, META, AMA(MØ), and AMA(LD) between XL and nonXL samples except the irradiation. *In vivo* UV-crosslinking was performed using the LT40 "Minitron" system (UV03 Ltd.) (24). Cells at 5 × 10^6 cells/ml confluence (~0.6 OD) were irradiated for 120s (Fig. 2*B*; ~1.6 mJ/cm^2) for optimal *in vivo* RBP:RNA (mRNP) crosslinking with superior mRNA integrity and negligible heat stress compared with a standard Stratalinker which exposes the cells to 100× the heat (~150 mJ/cm^2) (24). Both AMA(MØ) and AMA (LD) were irradiated in host MØs, which were then homogenized to release parasites for gradient purification as above.

Triplicate samples of ~5 × 10^9 cells of each lifecycle stage (XL and nonXL) were resuspended in 15 ml Lysis buffer (25) (20 mM Tris-HCl, pH7.5, 500 mM LiCl, 0.5% LDS, 1 mM EDTA and 5 mM DTT with cOmplete EDTA-free Protease Inhibitors ™ (Roche)) for 10 min at 0 °C, passed through a 25G needle until clear, centrifuged 10 min at 4000 × *g* and incubated with oligo(dT)$_{25}$ beads 30 min at 4 °C (New England Biolabs). Remaining steps for poly(A) RNA isolation were performed as described (18). mRNA-bound proteins were precipitated via TCA precipitation, and the resulting protein concentration measured using Micro BCA Protein assay kit (Thermo).

Label-free Quantitative Mass Spectrometry Analysis—

Trypsin Digestion—Triplicate biological samples were solubilized in NuPAGE LDS sample buffer (Life Technologies), heated at 70 °C for 10min and ran on a 7 cm NuPAGE Novex 10% Bis-Tris gel (Life Technologies) at 200 V for 6min. Gels were stained with SafeBLUE protein stain (NBS biologicals) for 1 h before destaining with ultrapure water for 1 h. In-gel tryptic digestion was performed after reduction with dithioerythritol and S-carbamidomethylation with iodoacetamide. Gel pieces were washed two times with aqueous 50% (v:v) acetonitrile containing 25 mM ammonium bicarbonate, then once with acetonitrile and concentrated in a vacuum for 20min. Sequence-grade, modified porcine trypsin (Promega) was dissolved in 50 mM acetic acid and diluted with 25 mM ammonium bicarbonate to give a final trypsin concentration of 0.02g/L. Gel pieces were rehydrated with 25 L of trypsin solution, incubated for 10 min then 25 mM ammonium bicarbonate solution was added to cover the gel pieces. Digests were incubated overnight at 37 °C. Peptides were extracted by washing three times with aqueous 50% (v:v) acetonitrile containing 0.1% (v:v) trifluoroacetic acid, before concentrating in a vacuum and reconstituting in aqueous 0.1% (v:v) trifluoroacetic acid. A common sample pool was created by taking equal aliquots of all samples.

LC-MS/MS—Samples were loaded onto an UltiMate 3000 RSLCnano HPLC system (Thermo) equipped with a PepMap 100Å C18, 5 μm trap column (300 μm × 5 mm Thermo) and a PepMap, 2 μm, 100Å, C18 EasyNano nanocapillary column (75 m × 150 mm; Thermo). The trap wash solvent was aqueous 0.05% (v:v) trifluoroacetic acid; trapping flow rate was 15 μl/min. The trap was washed for 3 min before switching flow to the capillary column. Separation used gradient elution of two solvents: solvent A, aqueous 1% (v:v) formic acid; solvent B, aqueous 80% (v:v) acetonitrile containing 1% (v:v) formic acid. The flow rate for the capillary column was 300 nL/min and the column temperature was 40 °C. The linear multistep gradient profile was: 3–10% B over 7 min, 10–35% B over 30 min, 35–99% B over 5min and then proceeded to wash with 99% solvent B for 4 min. The column was returned to initial conditions and re-equilibrated for 15min before subsequent injections. The nanoLC system was interfaced with an Orbitrap Fusion™ Hybrid™ mass spectrometer (Thermo) with an EasyNano ionisation source (Thermo). Positive

[1] The abbreviations used are: RBP, RNA binding proteins; mRNP, mRNA ribonucleoproteins; PCA, principal component analysis; PCF, procyclic promastigotes; META, metacyclic promastigotes; AMA, amastigotes; XL, Crosslinked; NoXL, Non-crosslinked; WC, whole cell.

ESI-MS and MS2 spectra were acquired using Xcalibur software (version 4.0, Thermo). Instrument source settings were: ion spray voltage, 1900 V; sweep gas, 0 Arb; ion transfer tube temperature; 275 °C. MS 1 spectra were acquired in the Orbitrap Fusion™ with: 120,000 resolution, scan range: *m/z* 375–1500; AGC target, $4e^5$; max fill time, 100 ms. Data-dependent acquisition was performed in top speed mode using a 1 s cycle, selecting the most intense precursors with charge states. Easy-IC was used for internal calibration. Dynamic exclusion was performed for 50 s post precursor selection and a minimum threshold for fragmentation was set at $5e^3$. MS2 spectra were acquired in the linear ion trap with: scan rate, turbo; quadrupole isolation, 1.6 *m/z*; activation type, HCD; activation energy: 32%; AGC target, $5e^3$; first mass, 110 *m/z*; max fill time, 100 ms. Acquisitions were arranged by Xcalibur to inject ions for all available parallelizable time.

Fusion PCR and Endogenous 3xHA Tagging of N Termini—For the generation of 3xHA N-tagged cell lines, the original modular pPOTv2 vector (26) was modified. The Ty-GFP-Ty tag was excised (HindIII/BamHI) and replaced by a 3xHA tag. Fusion PCR was performed as previously described. For transfections, 2×10^7 PCF cells were resuspended in Tb-BSF buffer (100 μl) and transfected (27). The parasites were selected with 10 μg/ml Blasticidin (Sigma).

RNA Coimmunoprecipitation and qRTPCR—HA-tagged RBPs were immunoprecipitated from PCF or META lysates with anti-HA magnetic beads (Thermo) coimmunoprecipitated RNA were extracted and measured via qRTPCR using SuperScript IV Reverse Transcriptase, Fast SYBR Green Master Mix and Quantstudio 3 PCR System (Thermo Fisher) as previously described (25). Relative levels of qRTPCRs were calculated via $2^{-\Delta\Delta Ct}$ using *nmt* as a constitutive control (28).

For the mRNA-bound capture experiment, the quality of the results was measured using depleted (*18S* ribosomal gene) and non-depleted (*nmt*) relative mRNA values before and after oligo$(dT)_{25}$-labeled magnetic bead purification. The relative levels were measured using the $2^{-\Delta Ct}$ method, using total RNA from samples before mRNA purification as a reference. The full list of primers used is provided in supplementary Table S3.

Western Blotting and Protein Expression—The different lifecycle stages of 3xHA endogenously tagged cell lines were grown and purified as described above. Parasites were lysed in Laemmli buffer and samples separated by SDS-PAGE, transferred to PVDF, labeled with anti-HA (1:10,000, Pierce) and anti-mouse IgG-HRP (1:50,000, Sigma) and developed using ECL (GE Healthcare). Relative protein expression was quantified using ImageJ software.

Data Analysis—Peak lists in .raw format were imported into Progenesis QI and LC-MS runs aligned to the common sample pool. Precursor ion intensities were normalized against total intensity for each acquisition. A combined peak list was exported in .mgf format for database searching against *L. mexicana* sequences appended with common proteomic contaminants (8365 sequences). Mascot-Daemon (version 2.5.1, Matrix Science) was used to submit the search to a locally-run copy of the Mascot program (Matrix Science Ltd., version 2.5.1). Search criteria specified: Enzyme, trypsin; Fixed modifications, Carbamidomethyl (C); Variable modifications, Oxidation (M); Peptide tolerance, 5 ppm; MS/MS tolerance, 0.5 Da; Instrument, ESI-TRAP. Search results were filtered to require a minimum expect score of 0.05. The Mascot .XML result file was imported into Progenesis QI and peptide identifications associated with precursor peak areas. Relative protein quantification was derived from unique peptide precursor ion intensities. Accepted quantifications were required to contain a minimum of two unique peptides. Statistical testing was performed in Progenesis QI and ANOVA-derived *p* values were converted to multiple test-corrected q-values using the Hochberg and Benjamini approach. Final quantification results were stripped of non-*Leishmania* spp. identifications for brevity.

TABLE I

RNA-bound versus Whole Cell proteome statistics and parameters. Statistics associated with WC and mRNA-associated (XL) Proteome comparisons of PCF, META and AMA lifecycle stage L. mexicana parasites (Fig 5*B*)

Lifecycle stage	UV crosslinked proteome vs whole cell proteome (simple linear model based on XL vs WC correlation)		
	Standard error (d.f.)	Adjusted R2	*p* value
All stages	3.959 (4,219)	0.0066	7.05E-08
PCF	2.956 (1,405)	0.0118	2.64E-05
META	4.051 (1,405)	0.1325	< 2.2E-16
AMA	3.486 (1,405)	0.0178	3.11E-07

Bioinformatics Analysis—

Comparison of Predicted Versus Isolated RBPomes—A list of characterized, published RNA binding domains was compiled from the InterPro database using manual curation and the search term "RNA binding." The 1407 isolated RBP candidates (1638 LC MS/MS protein identities) of the *L. mexicana* XL-RBPome were compared with the compiled list on Tritrypdb.org (08/2018) (29) using the "InterPro domain" function with the condition "intersect" (New search/Protein features and properties/InterPro domain). This same method of comparison was also completed between the compiled list and the whole *L. mexicana* protein coding genome. Diagrams were created with Microsoft Excel 2013, Corel Draw 2017 and Inkscape 0.92.3 softwares.

Venn Diagrams—WC and XL proteomes at each stage were filtered to include proteins with mean intensity values across each of the 3 replicates per condition intensity $\geq 10^6$. These proteins were used to create Venn diagrams in Python 2.7 using Matplotlib v.1.5.3 and Matplotlib-Venn package version 0.11.5.

Gene Ontology Term Analysis—Molecular Function GO Terms significantly enriched in the isolated mRBPome relative to the predicted *L. mexicana* proteome were derived using Tritrypdb.org (04.2017) (29). REVIGO software was used to refine and visualize enriched terms (revigo.irb.hr) (30).

Volcano Plots—Volcano plots were generated in Python 2.7 using Matplotlib v.1.5.3 and mpld3.js v.1.0 for interactive visualization. Log 2 fold-change values for every protein were calculated by taking the log 2 value of the ratio of mean intensity value + 1 between conditions. Independent *t*-tests were conducted using intensity values in each of the 3 replicates per condition to generate the *p* values used in the volcano plots.

Whole Cell Proteome Versus Transcriptome (31) Data Correlation—WC proteome and transcriptome correlations were made by averaging intensity values across replicates, using genes of q value ≤ 0.05 with at least 2 peptide hits. This was done for both the WC proteome *versus* the whole transcriptome, to identify any overarching correlations, and for each specific stage. For WC proteome and transcriptome comparisons, the ratio of PCF to AMA(MØ) intensity was calculated for each replicate, averaged and then $\log_2$ transformed. Genes obtained from the WC proteome were then compared with transcripts previously found to be differentially expressed between AMA(MØ) and promastigote^{log} stages (31). Intersecting genes between both datasets were then plotted against each other, using the ggplot2 R package, and the regressions fitted in Fig. 5*A* were modeled based on a loess linear model that derive the statistics in Table I below.

Following from this, the expression values from the proteomics data were then compared for each life cycle stage in both XL and WC

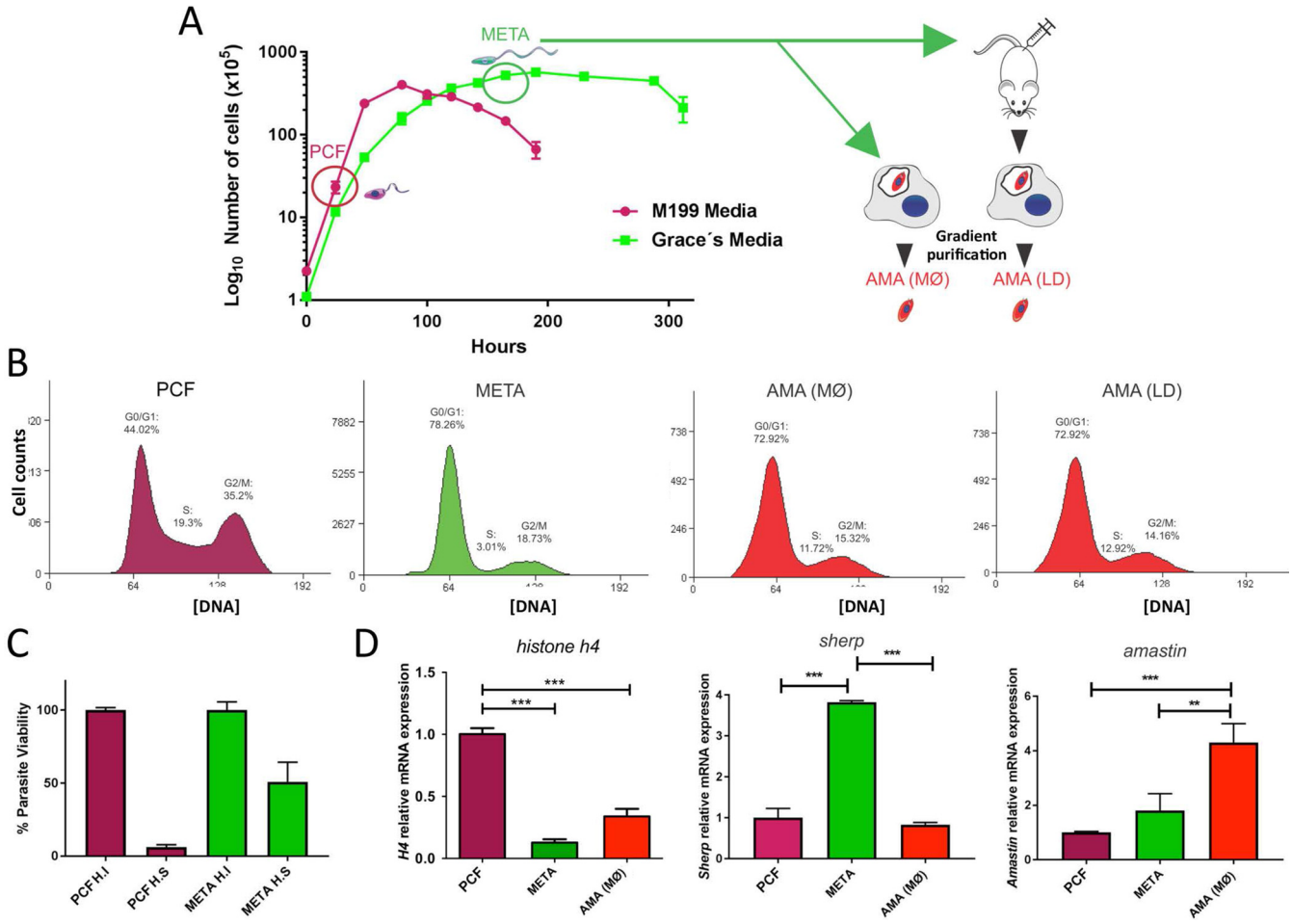

FIG. 1. **Isolation and validation of *L. mexicana* lifecycle stages**. *A*, Cumulative growth curve of *L. mexicana* in M199 (purple) and Grace's media (green). Harvested procyclic (PCF, purple circle) and metacyclic-enriched promastigote cultures (META, green circle) were tested for stage-specific traits. Metacyclic-enriched cultures were used to infect immortalized macrophages (J774.2 MØs) and mice to generate AMA (MØ) and AMA (LD) amastigote forms, respectively. Amastigotes forms (24 h post-infection (pi) for AMA (MØ) and 4 months pi for AMA(LD)) were gradient purified. *B*, FACS analyses compare DNA profiles of PCF, META, AMA (MØ) and AMA (LD) cells. Cell cycle profiles demonstrate PCF are highly proliferative, META are relatively quiescent and distinct AMA populations display a near-identical intermediate replicative capacity. *C*, Human serum resistance expressed as percentage parasite viability (*y* axis) of PCF (purple) and META (green) parasites treated with Human Serum (H.S) or Heat Inactivated human serum (H.I). *D*, Validation of each isolated *L. mexicana* stage by heightened mRNA expression of *histone h4*, *sherp* and *amastin* relative to *nmt* transcript levels presented as mean ± S.E. from 3 experimental replicates. One-way ANOVA and Tukey's post-test were conducted; $^{**}p < 0.01$, $^{***}p < 0.001$.

conditions. As before, the intensity values were averaged between replicates, and were plotted using ggplot2, however these were instead fit with a simple linear regression model, as a loess model did not improve the fit to the data.

Experimental Design and Statistical Rationale—Biological triplicates of each proteome sample (WC, XL, and nonXL) at all stages (PCF, META, AMA (Mø), and AMA(LD)) were quantitatively assessed for peptide ion enrichment. Data were searched against the TriTrypDB *Leishmania mexicana* proteome (version 8.1 - 30th Sep 2014, 8250 sequences; 5,180,224 residues) concatenated with 115 common proteomic contaminants including trypsin and human keratins (38,188 residues). Enzyme search parameters required full trypsin specificity (cleavage C-terminal to K or R not preceding P) and allowed for up to one missed cleavage. An identification false discovery rate of 2.4% was estimated empirically by searching against a reverse database and comparing the relative proportion of matches, restricting to the top scoring identification for each MS2 query and requiring a minimum of two unique peptides for each accepted protein.

RESULTS

Isolation and Validation of L. mexicana Life Cycle Stages—For the study of the different mRNA binding proteomes (mRBPomes) during the *L. mexicana* lifecycle, 4 biological samples corresponding to the 3 main lifecycle stages were isolated and molecularly verified. These were low passage (< P3), M199 media culture-derived procyclic promastigotes ("PCF"), Grace's media culture-derived metacyclic promastigotes ("META"), 24 h post-infection (24 h pi) macrophage-derived amastigotes ("AMA(MØ)") and *in vivo* lesion-derived amastigotes ("AMA(LD)"; Fig. 1*A*). Parasite cells were validated for specific lifecycle stages using distinct molecular markers and biologically-distinguishing features including cell cycle replicative status, resistance to human serum lysis and marker

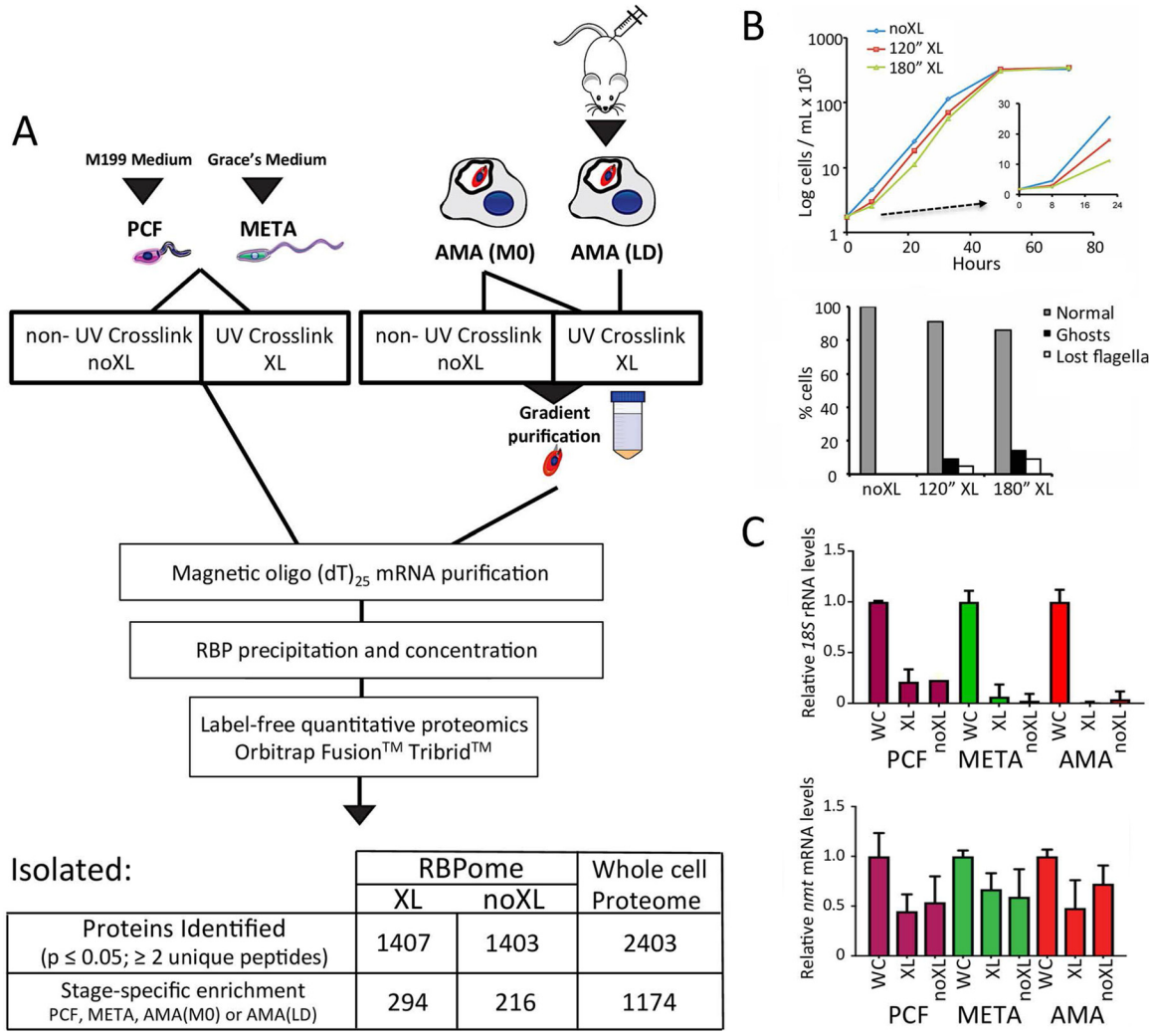

Isolated:

	RBPome XL	RBPome noXL	Whole cell Proteome
Proteins Identified ($p \leq 0.05$; ≥ 2 unique peptides)	1407	1403	2403
Stage-specific enrichment PCF, META, AMA(M0) or AMA(LD)	294	216	1174

FIG. 2. **Overview of the mRNA-interactome capture workflow.** *A*, *Leishmania* cells from verified lifecycle stages are UV-irradiated *in vivo* creating covalent bonds between mRNA and bound proteins in crosslinked (XL) *versus* non-crosslinked cells (nonXL). Cells are then purified, lysed and mRNP complexes are isolated using oligo(dT)-labeled magnetic beads. Isolated RBPs were precipitated and processed for label-free, quantified mass spectrometry. Numbers indicate identified proteins filtered for triplicate-consistent, high quality reads with at least 2 unique peptides. *B*, Growth curve and cell morphology after 120" or 180" UV-irradiation with optimized equipment. *C*, Relative RNA recovery of *18S* and *nmt* transcripts after oligo(dT) magnetic bead mRNA purification in XL, nonXL and WC lysates in PCF (purple), META (green) and AMA (MØ; red) samples.

gene expression (Fig. 1*B*–1*D*). The cell cycle analysis of PCF cell cultures mid-log at 5×10^6 cells/ml showed high replication efficiency (S: 19%, G2/M: 35%), sensitivity to human serum incubation and heightened *Histone h4* (*h4*) transcript expression (Fig. 1*B*, 1*C*, and 1*D*). We introduce *Histone H4* (*LmxM.36.0020*) here as a novel transcript marker of PCF stage *L. mexicana* parasites, investigated because of its specific expression in sandfly-derived *L. major* PCF cells (32). Stationary META form parasites were harvested at $\sim 4 \times 10^7$ cells/ml 7 days postincubation in Grace's media as described (20) and validated by reduced replication and protein synthesis (21) (S: 3%; G2/M: 19%), resistance to human complement lysis (33) and heightened expression of *sherp* transcript (22) (Fig. 1*B*, 1*C*, and 1*D*). Intracellular amastigote-stage parasites were isolated 24 h post-infection (24 h.p.i.) of cultured J774.2 macrophages, AMA(MØ), or from mouse rump lesions 4 months post-inoculation (23), AMA(LD), with serum-resistant META cells and gradient-purified as described (Experimental Procedures) (6). The 24 h.p.i. timing was selected as RNA levels are remodeled and differentiation into AMA(MØ) forms in the lysosomal environment is nearly complete (31). Purified amastigote-stage parasites were validated by electron microscopy (data not shown), heightened *amastin* (*LmxM.08.0840*) mRNA expression and cell cycle analysis that showed increased replication efficiency relative to META cells (Fig. 1*B* and 1*D*). Remarkably, FACS analysis of AMA(MØ) and AMA(LD) showed near-identical cell cycle profiles, intermediate between PCF and META replication efficiencies (Fig. 1*B*).

In Vivo Capture of L. mexicana RBPs—Fig. 2*A* illustrates the procedure used to isolate the mRBPomes. Indeed, up to

91% of cells showed wildtype morphology post-UV crosslinking (XL) with a small portion of non-crosslinked (nonXL) parasites able to restore culture growth after 120 s irradiation (Fig. 2*B*). Thus, this length of UV-exposure was selected for the mRNA-interactome capture experiments, with the mRNA subsequently isolated as previously described (18). All experimental conditions were optimized for large-scale harvests to isolate enough mRNA bound proteins (RBPs) for reliable, quantitative mass spectroscopy for each replicate. To round these analyses, relative enrichment of the mRBPomes were compared with whole cell (34) proteomes from each lifecycle stage; PCF, META, AMA(MØ). All peptide pools were evaluated simultaneously in triplicate on the Orbitrap Fusion™ mass spectrometer to quantitatively determine relative intensities of peptides in the mRBPomes and WC proteomes. The purity of the oligo(dT)-derived XL and nonXL mRNA was evaluated by relative elution of *18S* ribosomal RNA compared with the constitutively-expressed *N-myristoyltransferase* (*nmt; LmxM.31.0080*) mRNA as reference for overall mRNA recovery (Fig. 2*C*) (28). The results show a negligible amplification of *18S* rRNA relative to input and a substantial fraction of the *nmt* mRNA recovered after poly-A RNA isolation.

Whole Cell and RNA-bound Proteomes of the Main Leishmania Lifecycle Stages—The captured RBP peptides were analyzed by high-resolution mass spectrometry with a filter minimum of 2 unique peptides identified per protein and quantified using peptide precursor ion intensities ($p \leq 0.05$). A total of 1407 RBPs were identified in the XL samples (PCF, META, AMA(MØ), AMA(LD)) with 294 proteins significantly enriched at distinct stages, whereas 1403 RBPs were isolated from the nonXL peptide samples (PCF, META, AMA(MØ)) with 216 proteins displaying stage-specific association (Fig. 2*A*). This number is consistent with current RBP numbers in other eukaryotic systems (15). The RBPomes of 4 distinct *Leishmania* lifecycle stages have been pooled; equivalent to 4 distinct mammalian cell types, and our experimental method removes potential competition and quantitative limitations introduced by ion labeling (Experimental Procedures). In addition, mass spectrometry of whole cell (34) *L. mexicana* proteomes of each stage (PCF, META, AMA(MØ)) yielded 2403 proteins identified, 1174 of which are significantly enriched at one lifecycle stage (Fig. 2*A*). These data are available in supplementary Table S1. Confirming the integrity of our proteomes, principal component analysis (PCA) using relative protein quantification derived from unique peptide intensities was used to examine relatedness between the different biological samples and the variability among replicates (Fig. 3*A*). Notably, the triplicate proteomic samples cluster within discrete lifecycle stages for XL, nonXL, and WC proteomes displaying low variance among replicates and reproducibility of the results (Fig. 3*A*). These data infer reliable and distinct protein enrichment and identities for each lifecycle stage. In accordance with the FACS analyses of Fig. 1*B*, the PCA values for the AMA(LD) XL mRNA binding proteome is most like that of the AMA(MØ) XL, validating the use of AMA(MØ) for subsequent mRNP analyses. When combined, the WC proteomes cluster separately compared with the XL and nonXL mRBPomes, indicating that the isolated RBPs represent an enriched fraction with distinct relative intensities from that of the whole cell proteomes (supplementary Fig. S1*A*). Supporting the validity of the mRBPome, PCA analyses indicate the total proteomes, regardless of lifecycle stage, are more like each other in peptide identities and intensities than to any of the mRNA-selected proteomes (mRBPomes).

The specificity of our RNA binding proteomes (XL, nonXL) relative to the whole cell (34) proteome are further confirmed by Gene Ontology (GO) term enrichment analyses which demonstrate that significantly-enriched terms ($p \leq 0.05$) from the Molecular Function subset were reliably RNA-related; restricted to ribosomal components, RNA-binding and nucleic acid-binding with translation-related factors ranking somewhat less significantly (Fig. 3*B*). Despite a somewhat abridged proportion of annotation for the *L. mexicana* proteome, with 519 of the 1410 RBPs being hypothetical proteins, known protein identities within the isolated total mRBPome indicate appropriate enrichment.

Of interest, the number and identities of the RBPs within the XL *versus* nonXL mRBPome samples are remarkably similar, yet the relative peptide intensities are differentially-enriched (supplementary Fig. S2). This differential enrichment is because of the strength of RBP assocation in the XL samples being based on the number of covalent bonds formed when direct amino acid:mRNA interactions are irradiated (254 nm) whereas the nonXL protein:mRNA associations are reliant on the relative affinity of each RBP for mRNA (24). Accordingly, although the overall XL proteome is greatly enriched ($\geq$ 10 fold) relative to the nonXL samples, the nonXL RBPome is enriched for RNA helicases which exhibit particularly strong binding in clamped conformation (35). The fact the protein identities are overwhelmingly conserved between the XL and nonXL RBPomes supports the biological relevance of our results and deviates from previous kinetoplastid studies, which have used the nonXL samples as negative controls (16). Refined UV-crosslinking combined with the high sensitivity of the Orbitrap Fusion™ mass spectrometry system enables a deeper, quantified identification of nonXL without competing with the more abundant XL RBPome. Importantly, running each sample independently, label-free and concurrently prevented peptide competition for ion labeling and signal quenching, enabling quantitative comparison despite the significantly higher overall intensities of the XL *versus* the nonXL mRBPome samples. We further verified the stringency of all mRNA harvests (WC, XL and nonXL) through the lack of contaminating rRNA levels (Fig. 1*C*).

Proteomic Comparisons Reveal Stage-specific Distinctions—Filtered WC, nonXL and XL proteomes of each stage were compared using $\log_2$ fold change of peptide ion inten-

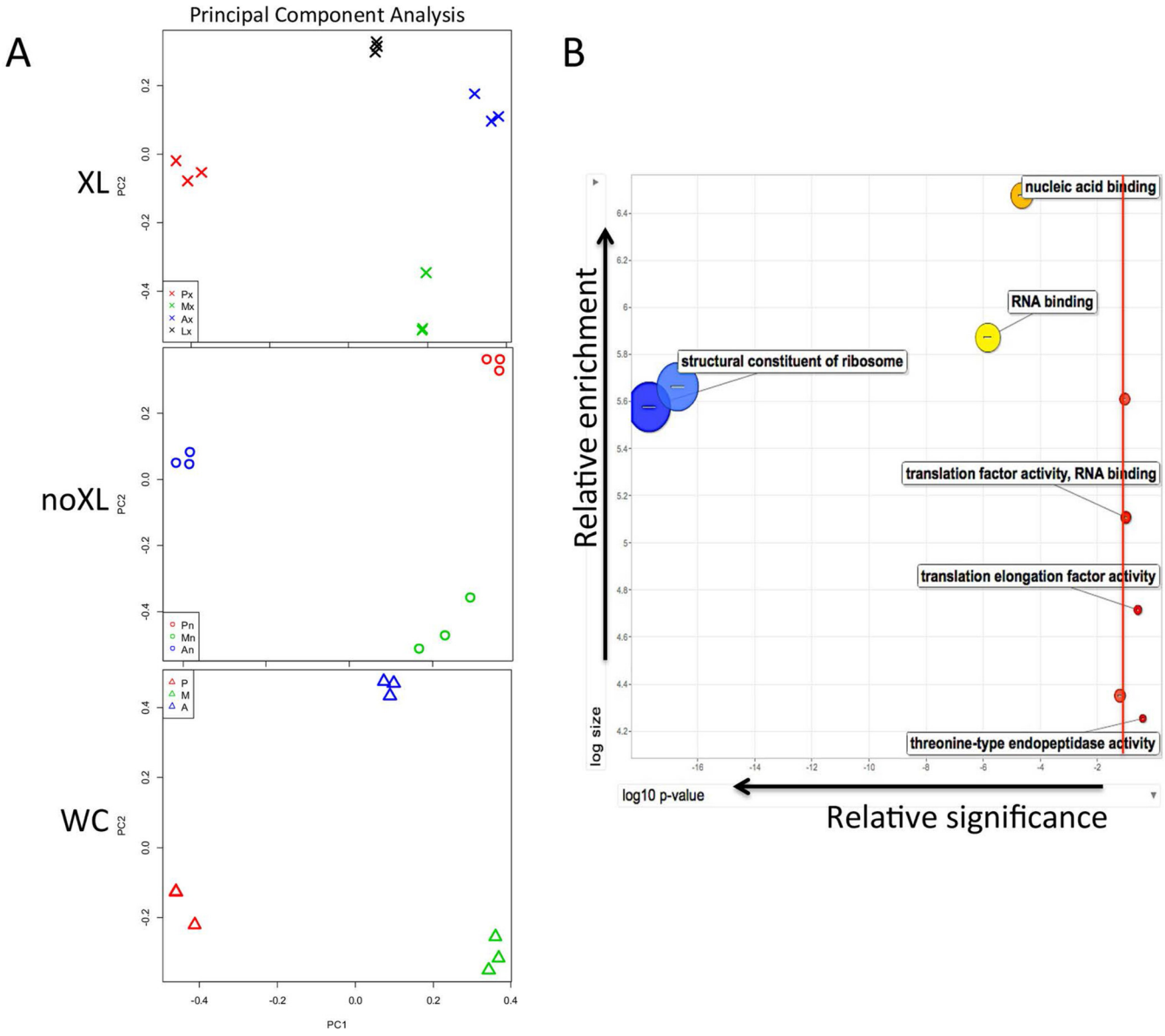

FIG. 3. **Variability and GO term enrichment among proteomes.** *A*, Principal component analysis (PCA) using relative protein quantification derived from unique peptide intensities was used to examine relatedness between the different biological samples and the variability among replicates. Notably, the triplicate proteomic samples cluster within discrete lifecycle stages for XL, nonXL and WC proteomes displaying low variance among replicates and reproducibility of the results. Colors indicate lifecycle stage of samples: PCF (red), META (green), AMA(MØ) (blue) and AMA(LD) (black). XL Samples (X) are Px = PCF XL, Mx = META XL, Ax = AMA(MØ) XL and Lx = AMA (LD) XL. NonXL Samples (O) are Pn = PCF nonXL, Mn = META nonXL and An = AMA(MØ) nonXL. WC Samples (Δ) are *p* = PCF WC, M = META WC and A = AMA(MØ) WC. *B*, Within the specific 234 RBPs Gene Ontology (GO) term enrichment analyses again indicated that this specific *L. mexicana* subset was enriched in the following terms by the following order: structural constituent of the ribosome ($p = 4.67e^{-10}$), RNA-binding ($p = 1.25e^{-6}$), nucleic acid binding ($p = 7.2e^{-4}$) indicating that the Molecular Function subfraction specific to the *L. mexicana* RBPome is overwhelmingly enriched in RNA-related terms. Red line indicates $p \leq 0.05$.

sities $\geq 10^6$ among biological samples to isolate factors which are stage-specifically enriched (supplementary Fig. S2). Importantly, filtering by intensity enables visualization of distinct protein enrichment but potentially excludes functionally-relevant proteins below this threshold. Comparison of the WC proteomes yielded 69, 50, and 27 proteins which are specifically enriched in PCF, META or AMA(MØ) stage parasites, respectively, with the majority common to all lifecycle stages. In contrast, most mRNA binding proteins are not common to all lifecycle stages but are differentially enriched and stage-regulated in both the nonXL and XL RBPomes (supplementary Fig. S2*A*). A complementary way of examining this data is provided in supplementary Fig. S2*B*; which compares the same protein enrichment analy-

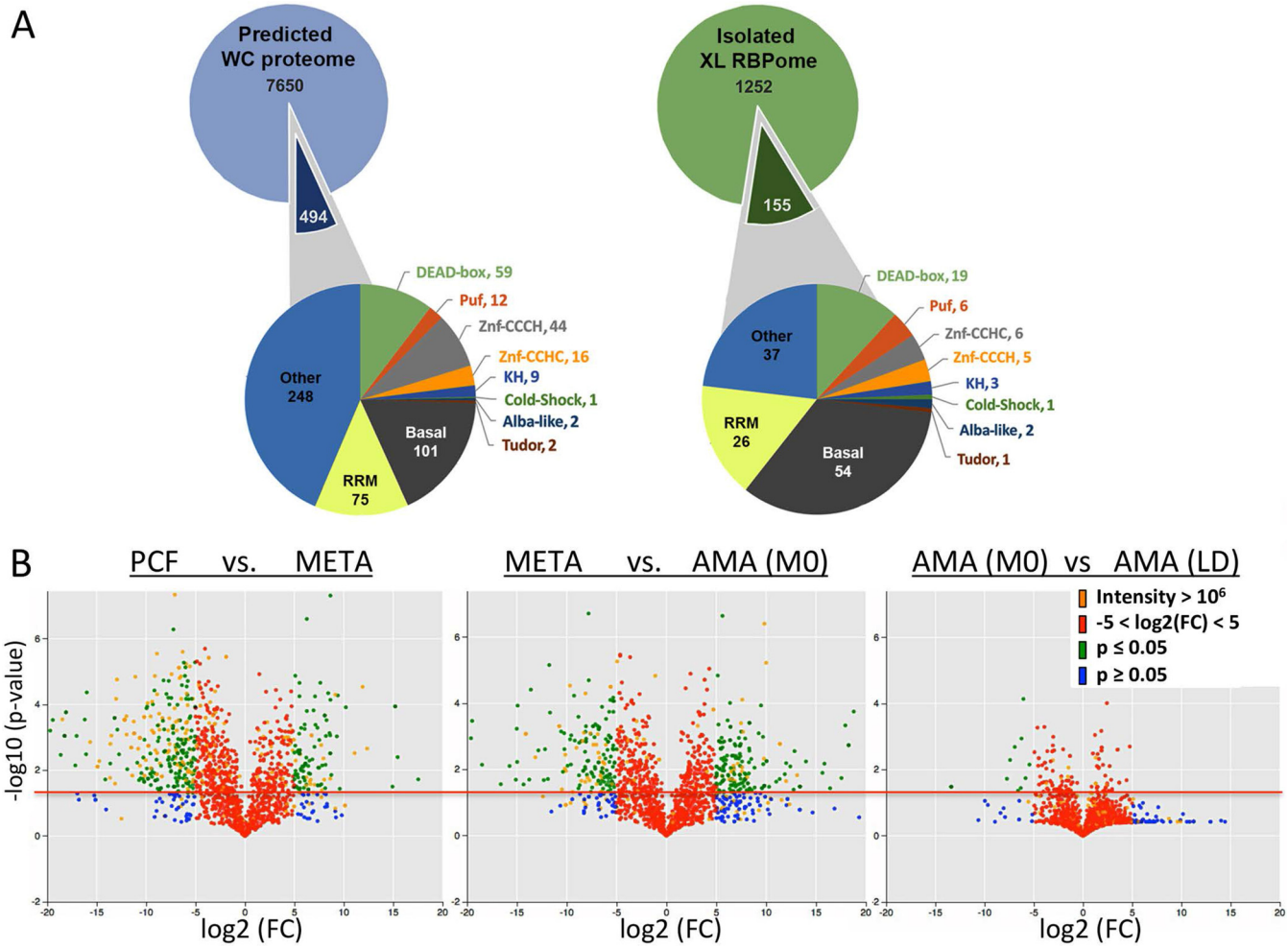

FIG. 4. ***L. mexicana* lifecycle whole cell and RBPome comparisons**. *A*, The number of proteins containing common RNA-binding domains (RBDs) in the predicted *L. mexicana* proteome (Tritrypdb.org) and XL-RBPome are presented. 494 out of 8144 genes in the total proteome and 155 out of 1407 proteins in the XL-RBPome contain known RBDs. Domain classes labeled as "Other" represent proteins with either additional, less abundant RBDs not listed separately in the diagram or weak conservation of known RBDs and "Basal" proteins have homology to the translational and splicing machinery. The RBPome RBD total is higher than the number of RBPs identified because of the presence of multiple domain classes in single proteins. *B*, Volcano plots were generated in Python using *p* values derived by conducting independent t-tests (3 replicates in stage 1 *versus* 3 replicates in stage 2). No multiple testing was conducted as the plots are for data visualization. The $\log_2$(FC) is $\log_2$((mean exp. condition 2 + 1)/(mean expression condition 1 + 1)). Red line indicates $p \leq 0.05$; protein identities above are significantly enriched in one lifecycle stage. Blue circles indicate identities below this threshold, green above. Red circles indicate proteins in the range of $-5 < \log_2(FC) < 5$ and orange circles indicate highly expressed factors with intensities $\geq 10^6$.

ses of the WC, XL and nonXL proteomes of each lifecycle stage (supplementary Fig. S2*B*).

Comparison between the predicted RBD-containing proteome of the *L. mexicana* genome (tritrypdb.org) and the isolated RBPome (XL) highlights some interesting distinctions (Fig. 4*A*). A significant reduction of zinc-finger domain proteins is evident in the isolated RBPome; with a 50% decrease in CCCH domain protein enrichment from 8% to 4%. This is consistent with the relative "silence" of zinc finger proteins in mass spectroscopy. Supporting the specificity of our data, the mRBPomes isolated from the highly replicative PCF stage displayed a large increase in the number of RBPs homologous to basal translational machinery. Overall, only 31% of the predicted proteins with RBDs in the whole genome are detected in our RBPome. The most likely explanation for this are the multiple timepoints within the *L. mexicana* lifecycle and *in vivo* conditions beyond the scope of this study.

To more closely compare the mRNA-bound proteomes between lifecycle stages without the exclusion of RBPs with lower intensities, XL proteomes of each stage were examined using $\log_2$ fold change of peptide ion intensities (Fig. 4*B*). Volcano plots represent the change in abundance (*x* axis) *versus* significance (*y* axis) of individual RBPs captured among the XL biological samples (Fig. 4*B*). The proteins of intensity $\geq 10^6$ that are analyzed in Fig. 4*A* can be observed here in orange *versus* the remaining identities. What is evident

is that these proteins of intensity $\geq 10^6$ make up the minority of protein identities overall, with identities above the red line displaying significantly distinct association with mRNA between the compared lifecycle stages. Identities in green have reduced intensities ($\leq 10^6$) but larger stage-specific shifts in protein bound to mRNA ($\log_2$(FC) < -5 or > 5). Consistent with the high division rate characteristic of the PCF stage (Fig. 1*B*), the PCF-specific XL RBPome is enriched for factors implicit in translation relative to the quiescent META stage XL mRBPome. Interestingly, large distinctions in relative enrichment are observed between the XL RBPomes enriched in META *versus* AMA(MØ), which are temporally separated by only 24 h. These RBPs are likely implicit in the differentiation potential (36) and initiation AMA(MØ) of amastigogenesis. Remarkably, the AMA stage samples display the least distinction of the XL mRBPomes despite the different host environments of an immortalized macrophage cell line *versus* an *in vivo* lesion 4 months post-infection (Fig. 4*B*). This finding contrasts the Venn Diagram comparison of the highly enriched AMA(MØ) and AMA(LD) RBPomes (Fig. 4*A*) and suggests that although the identities of a minority of highly enriched factors (intensities $> 10^6$) are distinct, the overall RBPomes of AMA(MØ) and AMA(LD) are remarkably similar. Combined with the near-identical cell cycle profile (Fig. 1*B*), the volcano plot profiles of AMA(MØ) and AMA(LD) (Fig. 4*B*) support cultured macrophages (MØs) as a useful model to investigate potential *trans*-regulators of *L. mexicana* differentiation *in vivo*.

mRNA and Protein Expression Versus RNA-binding Activity of RBPs—To validate proteomic results biochemically, specific RBPs of interest were endogenously HA-tagged on the N terminus to examine expression dynamics as controlled by endogenous 3′UTRs. Western blots confirmed stage-specific protein expression that corresponds with mass spectrometry results for RBP16 and UBP1 (supplementary Fig. S3). Compared with mRNA expression, protein expression of these RBPs displayed interesting variances. Although DRBD2 shows a relatively close correlation between transcript and protein levels, levels of SUB2, RBP16, DRBD3 and UBP1 proteins do not correspond well to encoding transcript levels (supplementary Fig. S3).

This led to a comprehensive examination of the previously observed phenomenon that *Leishmania* spp. protein and mRNA levels do not closely correspond (7). Given the scale of our proteomic results, we were able to use a GLM (Generalized Linear Model) of loess algorithm fit with a sliding window approach to visualize potential correlation between our WC (Purple) and XL (Green) proteomic data relative to published transcriptomic data (31) in both AMA(MØ) and PCF lifecycle stages (Fig. 5*A*). This comparison was limited to two lifecycle stages because of the transcriptome data available (31), however the low overall Pearson's correlation values indicate that neither the whole cell ($R^2 = 0.14$) nor RNA-bound ($R^2 = 0.0057$) proteome intensities correspond to levels of transcript expression. Although a stronger correlation between transcriptomic and whole cell proteomic data is evident in PCF stage cells which are more translationally active than AMA (Fig. 1*B*), there is negligible connection between the transcript expression of an RNA bound protein and its subsequent association with RNA (Fig. 5*A*). These results indicate that in *L. mexicana* parasites, RNA levels are not a strong predictor of whole cell expression or the RNA binding potential of proteins.

This comparison stimulated the question of how well WC RBP expression correlates to RNA binding potential (XL). Fig. 5*B* illustrates a linear regression fit (Lm [WC~XL]) to examine the RNA binding potential (XL RBPome; X-axis) of proteins quantified in our whole cell protein expression (WC RBPome; *y* axis) which meet XL/WC ratio Lm [WC~XL]. As our methods do not exclude the isolation of the translational machinery in our investigation, the high expression levels of translation factors influence this proteomic analysis. Although stages with high replication rates indicate a stronger correlation between protein expression (34) and RNA binding (XL), overall the correlations are lower than expected (Fig. 5*B*). Data from Figs. 1*B* and 4*B* also display influences relevant to translational activity as AMA cells are intermediary between PCF and META in both replication and translational efficiency with little correlation between RNA binding protein expression (34) and RNA association (XL) in the translationally-repressed, quiescent META stage parasites (Fig. 5*B*). These data indicate that expression of an RNA binding protein (34) is not a strong indicator of its RNA binding (XL). Importantly, this implies another level of regulation modulates or alters the RNA binding potential of RBPs. Given the strong evidence of stage-regulated post-translational modifications in this system (37), PTMs likely contribute to RNA binding potential.

Validation of Novel RNA Binding Proteins in L. mexicana—To functionally validate our mRBPome, multiple RBP candidates previously-uncharacterized in *Leishmania mexicana* were endogenously tagged (Fig. 6*A*), RNA immunoprecipitated (RIP) and associating transcripts were sequenced (data not shown). Top putative target transcripts for each RBP were validated and examined for stage-specific association by additional RIPs (Fig. 6*A*) and subsequent qRTPCRs of whole cell (Fig. 6*B*) *versus* RBP-associated transcript levels (Fig. 6*C*) in both PCF and META stage parasites. As expected, candidate RBPs associate with specific pools of transcript targets and this association can be stage-regulated. Of interest, some transcript targets are shared between RBPs and stage-specific fluctuations in mRNA-affinity can be target-specific. Remarkably, one of the more interesting RBP candidates, GAPDH protein, is expressed at relatively constant levels between PCF and META stage parasites yet selects distinct transcript target pools in these stages. This may suggest that the availability of a given RBP to bind mRNA can be altered in a bespoke manner to adjust its specificity, rather than a simple fluctuation in RNA binding capacity, in a stage-specific manner. Alternatively, and not exclusively, it may be that the

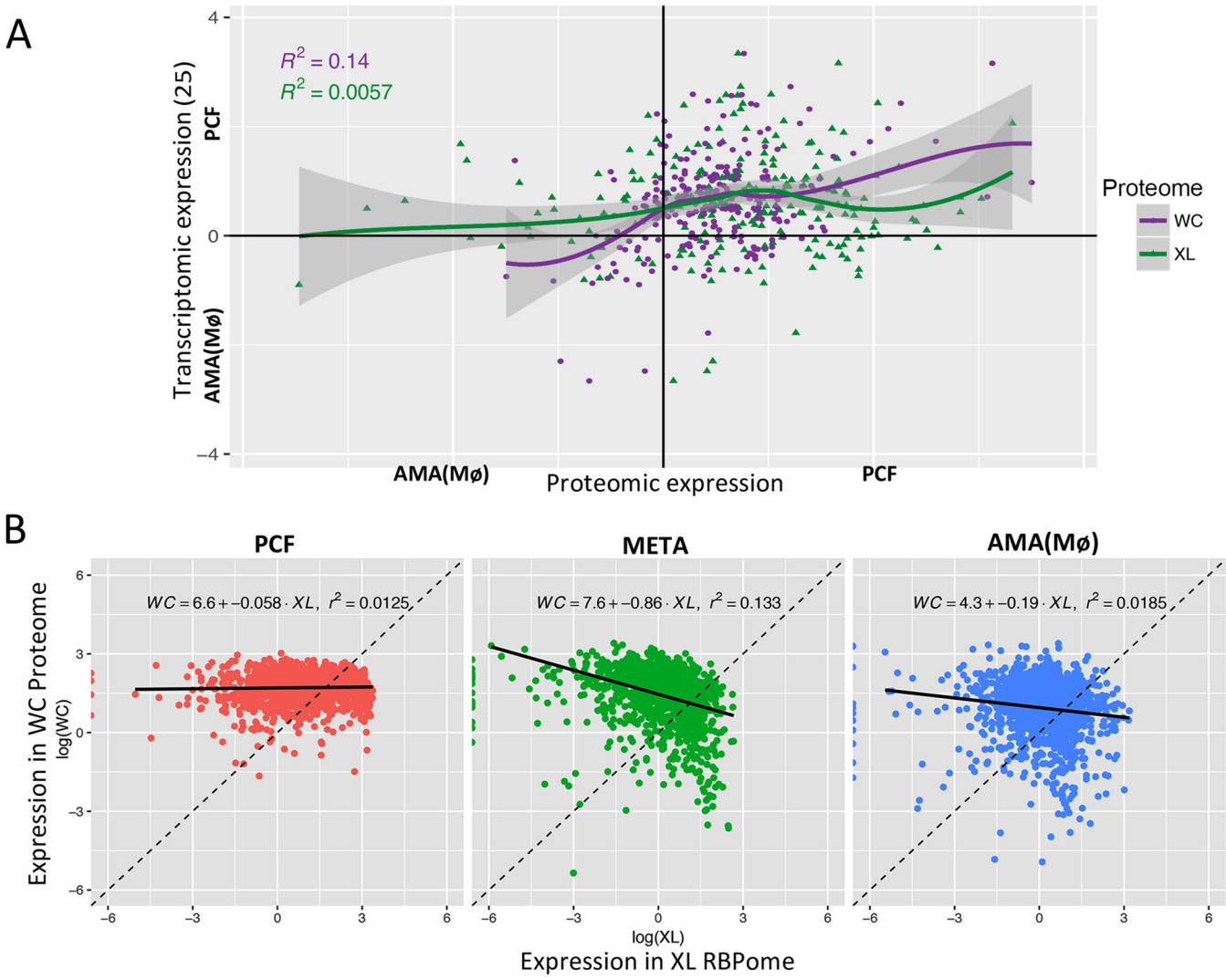

FIG. 5. **Comparing *L. mexicana* WC and XL Proteomes to Transcriptome data.** *A*, GLM (Generalized Linear Model) of loess algorithm fit displaying a sliding window approach to visualize relative correlation between the WC (Purple) and XL (Green) proteomic data relative to published *L. mexicana* transcriptomic data (30) in AMA(MØ) *versus* PCF lifecycle stages. Gray shading = S.E. Relevant statistics provided in Table I. *B*, A linear regression fit against all proteins which meet XL/WC ratio, Lm [WC∼XL]. Expressed proteins are more likely to bind mRNA in PCF than META with AMA intermediary. Likelihood for expressed proteins to bind RNA correlates well to both replicative and translational efficiency of each lifecycle stage.

structure and exposure of regulatory elements within mRNA targets change during the lifecycle. Overall, this molecular data supports and extends our bioinformatic findings that the whole cell expression of an RNA binding protein in a given lifecycle stage does not guarantee its association with target transcripts. Instead, RBP expression merely establishes the potential to bind and regulate mRNA, which is then subject to cellular context.

DISCUSSION

Gene regulation in *Leishmania* spp. parasites is overwhelmingly post-transcriptional as genes are constitutively transcribed in polycistronic tandem arrays (2). Despite a strong emphasis on *trans*-regulators as the primary gene regulators, remarkably few have been characterized or validated in these parasites. Here we present a comprehensive, quantitative list of the mRNA-bound proteomes as well as the whole cell proteomes of the 3 main lifecycle stages; procyclic promastigotes, metacyclic promastigotes and amastigote stage *L. mexicana*. We isolated and molecularly validated distinct stages via published criteria including growth in bespoke media, replication efficiency, relative resistance to human serum complement and heightened expression of stage-specific gene markers (20–22, 33). As a result, we present a comprehensive, updated method for obtaining large quantities of validated, distinct *L. mexicana* lifecycle stages that provide useful insight for the research community. The proteomes of different stages display remarkable protein expres-

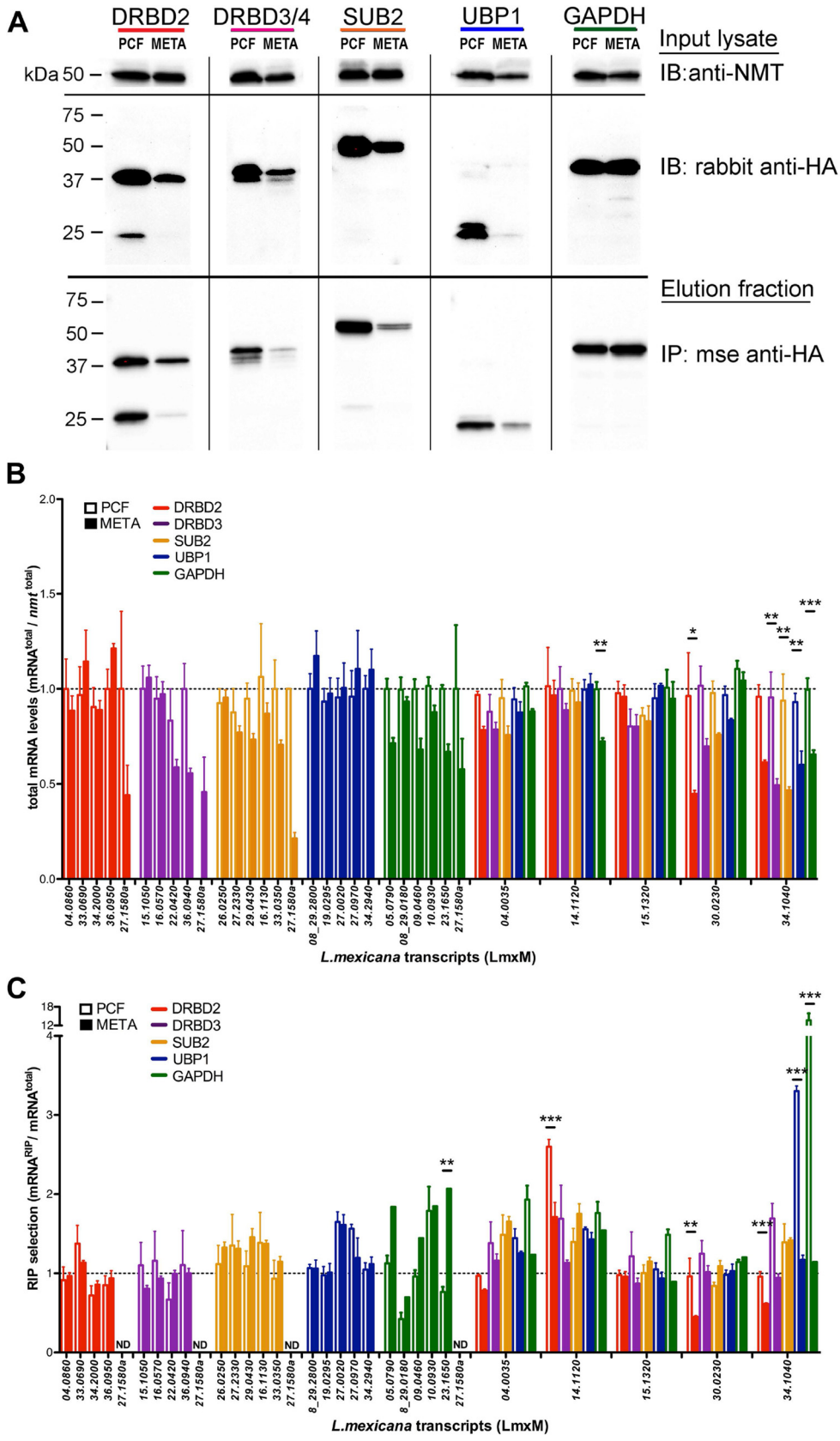

sion diversity in line with the different environments they inhabit. Cell-type specific gene expression is particularly common in parasites as a protein that is key for survival in one lifecycle stage may represent a vulnerability in the next. We present here the foremost comprehensive RNA binding (XL, nonXL) and whole cell (34) proteomes yet available in *Leishmania* parasites as a significant resource for the research community.

Several publications have previously described lifecycle-specific proteomes in *Leishmania* spp. parasites (6, 7). Notably, Paape *et al.* previously published proteomes derived from logarithmic promastigote and macrophage-derived amastigote stage *L. mexicana* in search of potential virulence factors (6). This study identified enriched octomers within 3′*UTR*s that may contribute to stage-specific protein expression. Further to this, a direct comparison by Lahav *et al.* observed that transcriptomes of axenic *L. donovani* promastigotes and amastigotes did not correspond to proteomic data, except during the first hour of axenic amastigogenesis (7). Our data (Fig. 5*A*) supports this finding albeit on a broader timescale than an hourly time-course and in a different *Leishmania* species, suggesting this lack of correlation between mRNA and protein expression may be common to all *Leishmania*. Certainly transcript expression potentiates *Leishmania* protein expression and thereby provides useful insight into gene expression that would be prohibitively expensive and experimentally challenging to obtain on the proteomic level currently (32).

Recently, there have been two RBPome studies in kinetoplastid parasites which isolated 128 RNA bound proteins from axenically-derived amastigote stage (AXA) *L.donovani* (17), and 155 RBPs from *T.brucei* monomorphic slender bloodstream form (BSF) parasites (16). These studies each examine a single, mammalian-infective form of the parasite. Direct comparisons between the RBPomes have caveats, given the large divergence between intracellular (*Leishmania*) *versus* extracellular (*T.brucei*) cells and different isolation methods involved. As the PCF, AXA, and BSFs are all proliferative stages, translation factors implicit in cell replication are common to all these RBPomes. Our data examines RBPome association dynamics through lifecycle progression using the foremost mass spectroscopy technology. This strategy revealed stage-specific modulation of RBP:mRNA associations indicative of a highly bespoke transcript target selection that is independent of expression levels. Indeed, this complicates the traditional RBP:transcript target paradigm in a meaningful, interesting manner with similarities to transcriptional context.

The scale and filters we have employed for our investigation select the most abundant proteins bound to mRNA. Accordingly, in addition to specific *trans*-acting gene regulators we have isolated the translational machinery of each lifecycle stage. Therefore, the relative replication and translational efficiency of each lifecycle stage has strongly influenced many of our RBPome comparisons; including the observed correlation between proteomic expression and mRNA association. Although it is beyond the scope of this study, our data provides significant direction toward *Leishmania* ribosomal analyses. Indeed stage-dependent distinctions in the translational machinery may impact general mechanisms, however the primary objective of these analyses is to identify mRNA-bound factors that regulate gene expression and promote differentiation to human-infective forms. That is, *trans*-regulatory RBPs which coordinate both developmental and virulence-promoting regulons.

Given the depth and sensitivity of our proteomics, we cannot rule out the possibility that some of our factors may be indirectly bound by tight protein/protein interactions with directly-bound RBPs. This may explain the presence of non-canonical RNA associating factors; the validity of which is supported by their consistent isolation in RBPomes from other organisms and the knowledge that the current list of RNA binding domains is not exhaustive (14, 16, 17, 38). The consistency and quality of our methods and results are evident in the near-match identities of our proteomes isolated from mRNA derived from both *in vivo* crosslinked and non-crosslinked cells of all lifecycle stages, negating artifactual RNA binding as a result of UV-crosslinking. Our analyses compare relative enrichment of factors within the Whole Cell *versus* mRNA-bound proteomes and found highly abundant proteins which also bind mRNA appear to be limited to ribosomal factors. Thus, we conclude that nonspecific background proteins were not isolated in our screen.

The data from Fig. 4*B* demonstrates META-specific factors bind RNA in large abundance and are distinct from PCF and AMA-enriched RBPs. The relative quiescence of this stage as evidenced by Figs. 1*B* and 5*B*, places extra emphasis on the potential importance of META-enriched RNA binding proteins as promoters of transmission to mammalian hosts and differentiation to AMA forms (39). Indeed, if the META stage cells cannot properly respond to environmental cues of a mammalian phagolysosome and differentiate to AMA stage, the lifecycle is halted and there is no infection or disease (2). Of interest as well are the RNA binding factors distinguishing META stage parasites from AMA(MØ) RBPs as the former

FIG. 6. **Validation of novel *L. mexicana* RBPs.** *A*, Western blots (anti-HA) of whole cell lysate (Input) and immunoprecipitations (Elution) of endogenously-tagged RBP candidates show specific isolation in both PCF and META stages. *B*, Whole cell expression of candidate transcript targets are shown in both PCF and META stages, normalized to *nmt* transcript expression. *C*, HA-RBP RIP-selected mRNA levels are shown relative to WC levels (*B*) for each target RNA. All qRTPCR data are presented as mean ± S.E. from 3 biological replicates. Two-way ANOVA test and Bonferroni between log and stationary phase samples indicate a stage-regulated association with target transcripts for some RBPs; $^{*}p < 0.05$, $^{**}p < 0.01$, $^{***}p < 0.001$. ND = Not Detected.

holds the potential to differentiate while the latter is in amastigogenesis (Fig. 5*B*). Similarly, mRBPs which are enriched in AMA(MØ) relative to AMA(LD) cells may provide further candidate *trans*-regulators that control amastigogenesis as AMA(MØ) is still in the process whereas AMA(LD) have been through multiple replication cycles within this lifecycle stage long term.

Comparison of the predicted RBD-containing proteome of the *L. mexicana* genome to the isolated RBPome highlights some interesting distinctions including a decrease in the proportion of some zinc-finger domain proteins and in the basal translational machinery, particularly in the replicative stages. There are several, non-exclusive potential explanations for this. The temporally-defined isolation of these RBPomes may limit the scope. Although the RBPome has data from 4 distinct lifecycle stages, there are at least 3 lifecycle stages (nectomonad, leptomonad and haptomonad promastigotes) and multiple differentiation events not examined here in which non-isolated RBPs might be transiently expressed. Zinc finger proteins characteristically display reduced detection via mass spectroscopy. A study isolating and examining the missing lifecycle stages and differentiation time courses could detect additional RBPs, but isolation of these less-defined stages from sandflies at the numbers required for mass spectroscopy is experimentally prohibitive. Despite these caveats, this study presents the largest scale isolation of RBPs to date in kinetoplastids with valuable information on the types of proteins associating with mRNA in these parasites. These proteomes lend insight into the dynamic cellular context in which *Leishmania trans*-regulators bind RNA, as well as potential modifying enzymes which control RBP behavior and function.

Important findings from this work include the low correlation of protein expression *versus* transcript expression, the stage-specific variation in protein expression *versus* RNA binding potential, and the modulation of RNA binding protein enrichment during the *Leishmania* parasite lifecycle. This is the first study to examine the whole cell or mRNA binding proteome of the metacyclic promastigote parasites essential for human transmission, infectivity and lifecycle progression. We endogenously tagged and molecularly verified the association of multiple RBP candidates with distinct, stage-regulated transcript target pools. Functional investigations into candidate regulators will undoubtedly isolate factors essential for parasite lifecycle progression, viability and transmission. As the majority of kinetoplastid proteins are not homologous to other systems, including mammals, *trans*-regulators that enable the parasite to adapt and survive in different environments may provide viable targets for anti-leishmanial treatments.

Acknowledgments—All the Proteomic work and part of the Bioinformatic analyses was conducted within the Bioscience Technology Facility (https://www.york.ac.uk/biology/technology-facility) at the University of York. UV-crosslinking was advised by David Tollervey and Sander Granneman. We would like to thank Deborah Smith, Alvaro Acosta-Serrano and Dawn Coverley for helpful comments on this manuscript.

DATA AVAILABILITY

Proteomic data sets are available to download from MassIVE (MSV000083023) and ProteomeXchange (PXD011340). All proteomic data has been submitted to TriTrypDB (http://tritrypdb.org/), which is possible through the collaborative efforts between EuPathDB, GeneDB and the Center for Infectious Disease Research (CIDR).

* This work was supported by the Medical Research Council [grant number MR/L00092X/1 to PBW]. Funding for open access charge: Medical Research Council and University of York. LCMS within the York Centre of Excellence in Mass Spectrometry was founded through Science City York and Yorkshire Forward/Northern Way Initiative; and is supported by EPSRC [grant numbers EP/K039660/1, EP/M028127/1].

§§ To whom correspondence should be addressed. E-mail: pegine.walrad@york.ac.uk.

‖ Current Address: Department of Parasitology, University of Granada, Spain.

**Current Address: National Institute of Allergy and Infectious Diseases, National Institute of Health, Bethesda, MD.

‡‡These authors contributed equally to this work.

Author contributions: L.M.D.P., T.R.F., A.D., E.P., and P.B.W. performed research; L.M.D.P., T.R.F., A.D., S.F., E.P., K.N., and P.B.W. analyzed data; L.M.D.P., T.R.F., A.D., S.F., E.P., and P.B.W. wrote the paper; A.D. and P.B.W. designed research; A.D., S.F., K.N., and P.B.W. contributed new reagents/analytic tools; P.B.W. supervised project.

Ethics statement: All animal procedures for this research have been passed by the University Animal Welfare Ethical Review Body (AWERB) and is carried out under the Home Office Project Licence [39_4377]. The University of York and the Home Office Project Licence meets all the standard conditions and works according to Codes of Practice under the under the Animals (Scientific Procedures) Act 1986 (Amended 2012).

REFERENCES

1. WHO (2017) W.H.O. Global leishmaniasis update, 2006–2015: a turning point in leishmaniasis surveillance. *WHO Weekly Epidemiolog. Rec.* **92,** 557–572
2. De Pablos, L. M., Ferreira, T. R., and Walrad, P. B. (2016) Developmental differentiation in Leishmania lifecycle progression: post-transcriptional control conducts the orchestra. *Curr. Opin. Microbiol.* **34,** 82–89
3. Bringaud, F., Muller, M., Cerqueira, G. C., Smith, M., Rochette, A., El-Sayed, N. M., Papadopoulou, B., and Ghedin, E. (2007) Members of a large retroposon family are determinants of post-transcriptional gene expression in Leishmania. *PLoS Pathog.* **3,** 1291–1307
4. Abanades, D. R., Ramirez, L., Iborra, S., Soteriadou, K., Gonzalez, V. M., et al. (2009) Key role of the 3′ untranslated region in the cell cycle regulated expression of the Leishmania infantum histone H2A genes: minor synergistic effect of the 5′ untranslated region. *BMC Mol. Biol.* **10,** 48
5. David, M., Gabdank, I., Ben-David, M., Zilka, A., Orr, I., et al. (2010) Preferential translation of Hsp83 in Leishmania requires a thermosensitive polypyrimidine-rich element in the 3′ UTR and involves scanning of the 5′ UTR. *RNA* **16,** 364–374
6. Paape, D., Barrios-Llerena, M. E., Le Bihan, T., Mackay, L., and Aebischer, T. (2010) Gel free analysis of the proteome of intracellular Leishmania mexicana. *Mol. Biochem. Parasitol.* **169,** 108–114

7. Lahav, T., Sivam, D., Volpin, H., Ronen, M., Tsigankov, P., Green, A., Holland, N., Kuzyk, M., Borchers, C., Zilberstein, D., and Myler, P. J. (2011) Multiple levels of gene regulation mediate differentiation of the intracellular pathogen Leishmania. *FASEB J.* **25,** 515–525
8. Cloutier, S., Laverdiere, M., Chou, M. N., Boilard, N., Chow, C., and Papadopoulou, B. (2012) Translational control through eIF2alpha phosphorylation during the Leishmania differentiation process. *PLoS ONE* **7,** e35085
9. Vasconcelos, E. J., Terrao, M. C., Ruiz, J. C., Vencio, R. Z., and Cruz, A. K. (2012) In silico identification of conserved intercoding sequences in Leishmania genomes: unraveling putative cis-regulatory elements. *Mol. Biochem. Parasitol.* **183,** 140–150
10. Dupe, A., Dumas, C., and Papadopoulou, B. (2014) An Alba-domain protein contributes to the stage-regulated stability of amastin transcripts in Leishmania. *Mol. Microbiol.* **91,** 548–561
11. Padmanabhan, P. K., Zghidi-Abouzid, O., Samant, M., Dumas, C., Aguiar, B. G., Estaquier, J., and Papadopoulou, B. (2016) DDX3 DEAD-box RNA helicase plays a central role in mitochondrial protein quality control in Leishmania. *Cell Death Dis.* **7,** e2406
12. Gehring, N. H., Wahle, E., and Fischer, U. (2017) Deciphering the mRNP code: RNA-bound determinants of post-transcriptional gene regulation. *Trends Biochem. Sci.* **42,** 369–382
13. Fritz, M., Vanselow, J., Sauer, N., Lamer, S., Goos, C., Siegel, T. N., Subota, I., Schlosser, A., Carrington, M., and Kramer, S. (2015) Novel insights into RNP granules by employing the trypanosome's microtubule skeleton as a molecular sieve. *Nucleic Acids Res.* **43,** 8013–8032
14. Beckmann, B. M., Horos, R., Fischer, B., Castello, A., Eichelbaum, K., Alleaume, A. M., Schwarzl, T., Curk, T., Foehr, S., Huber, W., Krijgsveld, J., and Hentze, M. W. (2015) The RNA-binding proteomes from yeast to man harbour conserved enigmRBPs. *Nat. Commun.* **6,** 10127
15. Hentze, M. W., Castello, A., Schwarzl, T., and Preiss, T. (2018) A brave new world of RNA-binding proteins. *Nat. Rev. Mol. Cell Biol.* **19,** 327–341
16. Lueong, S., Merce, C., Fischer, B., Hoheisel, J. D., and Erben, E. D. (2016) Gene expression regulatory networks in Trypanosoma brucei: insights into the role of the mRNA-binding proteome. *Mol. Microbiol.* **100,** 457–471
17. Nandan, D., Thomas, S. A., Nguyen, A., Moon, K. M., Foster, L. J., and Reiner, N. E. (2017) Comprehensive identification of mRNA-binding proteins of Leishmania donovani by interactome capture. *PLoS ONE* **12,** e0170068
18. Castello, A., Horos, R., Strein, C., Fischer, B., Eichelbaum, K., Steinmetz, L. M., Krijgsveld, J., and Hentze, M. W. (2016) Comprehensive identification of RNA-binding proteins by RNA interactome capture. *Methods Mol. Biol.* **1358,** 131–139
19. McKean, P. G., Denny, P. W., Knuepfer, E., Keen, J. K., and Smith, D. F. (2001) Phenotypic changes associated with deletion and overexpression of a stage-regulated gene family in Leishmania. *Cell Microbiol.* **3,** 511–523
20. Rogers, M., Kropf, P., Choi, B. S., Dillon, R., Podinovskaia, M., Bates, P., and Müller, I. (2009) Proteophosophoglycans regurgitated by Leishmania-infected sand flies target the L-arginine metabolism of host macrophages to promote parasite survival. *PLoS Pathog.* **5,** e1000555
21. Sacks, D. L., and da Silva, R. P. (1987) The generation of infective stage Leishmania major promastigotes is associated with the cell-surface expression and release of a developmentally regulated glycolipid. *J. Immunol.* **139,** 3099–3106
22. Depledge, D. P., Evans, K. J., Ivens, A. C., Aziz, N., Maroof, A., Kaye, P. M., and Smith, D. F. (2009) Comparative expression profiling of Leishmania: modulation in gene expression between species and in different host genetic backgrounds. *PLoS Negl. Trop. Dis.* **3,** e476
23. Coombs, G. H., Hart, D. T., and Capaldo, J. (1983) Leishmania mexicana: drug sensitivities of promastigotes and transforming amastigotes. *J. Antimicrob. Chemother.* **11,** 151–162
24. Granneman, S., Petfalski, E., Swiatkowska, A., and Tollervey, D. (2010) Cracking pre-40S ribosomal subunit structure by systematic analyses of RNA-protein cross-linking. *EMBO J.* **29,** 2026–2036
25. Walrad, P., Paterou, A., Acosta-Serrano, A., and Matthews, K. R. (2009) Differential trypanosome surface coat regulation by a CCCH protein that co-associates with procyclin mRNA cis-elements. *PLoS Pathog.* **5,** e1000317
26. Dyer P, Dean S, Sunter J. (2016) High-throughput Gene Tagging in Trypanosoma brucei. *J Vis Exp.* Aug **12**;(114)
27. Burkard, G., Fragoso, C. M., and Roditi, I. (2007) Highly efficient stable transformation of bloodstream forms of Trypanosoma brucei. *Mol. Biochem. Parasitol.* **153,** 220–223
28. Price, H. P., Guther, M. L., Ferguson, M. A., and Smith, D. F. (2010) Myristoyl-CoA:protein N-myristoyltransferase depletion in trypanosomes causes avirulence and endocytic defects. *Mol. Biochem. Parasitol.* **169,** 55–58
29. Aslett, M., Aurrecoechea, C., Berriman, M., Brestelli, J., Brunk, B. P., Carrington, M., Depledge, D. P., Fischer, S., Gajria, B., Gao, X., Gardner, M. J., Gingle, A., Grant, G., Harb, O. S., Heiges, M., Hertz-Fowler, C., Houston, R., Innamorato, F., Iodice, J., Kissinger, J. C., Kraemer, E., Li, W., Logan, F. J., Miller, J. A., Mitra, S., Myler, P. J., Nayak, V., Pennington, C., Phan, I., Pinney, D. F., Ramasamy, G., Rogers, M. B., Roos, D. S., Ross, C., Sivam, D., Smith, D. F, Srinivasamoorthy, G., Stoeckert, C. J. Jr, Subramanian, S., Thibodeau, R., Tivey, A., Treatman, C., Velarde, G., and Wang, H. (2010) TriTrypDB: a functional genomic resource for the Trypanosomatidae. *Nucleic Acids Res.* **38,** D457–D462
30. Supek, F., Bosnjak, M., Skunca, N., and Smuc, T. (2011) REVIGO summarizes and visualizes long lists of gene ontology terms. *PLoS ONE* **6,** e21800
31. Fiebig, M., Kelly, S., and Gluenz, E. (2015) Comparative life cycle transcriptomics revises Leishmania mexicana genome annotation and links a chromosome duplication with parasitism of vertebrates. *PLoS Pathog.* **11,** e1005186
32. Inbar, E., Hughitt, V. K., Dillon, L. A., Ghosh, K., El-Sayed, N. M., and Sacks, D. L. (2017) The transcriptome of Leishmania major developmental stages in their natural sand fly vector. *MBio* **8,** e00029-17
33. Puentes, S. M., Da Silva, R. P., Sacks, D. L., Hammer, C. H., and Joiner, K. A. (1990) Serum resistance of metacyclic stage Leishmania major promastigotes is due to release of C5b-9. *J. Immunol.* **145,** 4311–4316
34. Cheng, T. H., Thompson, D., Painter, J., O'Mara, T., Gorman, M., Martin, L., Palles, C., Jones, A., Buchanan, D. D., Win, A. K., Hopper, J., Jenkins, M., Lindor, N. M., Newcomb, P. A., Gallinger, S., Conti, D., Schumacher, F., Casey, G., Giles, G. G., Pharoah, P., Peto, J., Cox, A., Swerdlow, A., Couch, F., Cunningham, J. M., Goode, E. L., Winham, S. J., Lambrechts, D., Fasching, P., Burwinkel, B., Brenner, H., Brauch, H., Chang-Claude, J., Salvesen, H. B., Kristensen, V., Darabi, H., Li, J., Liu, T., Lindblom, A., Hall, P., de Polanco, M. E., Sans, M., Carracedo, A., Castellvi-Bel, S., Rojas-Martinez, A., Aguiar, Jnr, S., Teixeira, M. R., Dunning, A. M., Dennis, J., Otton, G., Proietto, T., Holliday, E., Attia, J., Ashton, K., Scott, R. J., McEvoy, M., Dowdy, S. C., Fridley, B. L., Werner, H. M., Trovik, J., Njolstad, T. S., Tham, E., Mints, M., Runnebaum, I., Hillemanns, P., Dörk, T., Amant, F., Schrauwen, S., Hein, A., Beckmann, M. W., Ekici, A., Czene, K., Meindl, A., Bolla, M. K., Michailidou, K., Tyrer, J. P., Wang, Q., Ahmed, S., Healey, C. S., Shah, M., Annibali, D., Depreeuw, J., Al-Tassan, N. A., Harris, R., Meyer, B. F., Whiffin, N., Hosking, F. J., Kinnersley, B., Farrington, S. M., Timofeeva, M., Tenesa, A., Campbell, H., Haile, R. W., Hodgson, S., Carvajal-Carmona, L., Cheadle, J. P., Easton, D., Dunlop, M., Houlston, R., Spurdle, A., and Tomlinson, I. (2015) Meta-analysis of genome-wide association studies identifies common susceptibility polymorphisms for colorectal and endometrial cancer near SH2B3 and TSHZ1. *Sci. Rep.* **5,** 17369
35. Iwasaki, S., Floor, S. N., and Ingolia, N. T. (2016) Rocaglates convert DEAD-box protein eIF4A into a sequence-selective translational repressor. *Nature* **534,** 558–561
36. Adare, A., Afanasiev, S., Aidala, C., Ajitanand, N. N., Akiba, Y., et al. (2015) Measurements of elliptic and triangular flow in high-multiplicity 3He+Au collisions at radical(s(NN))=200 GeV. *Phys. Rev. Lett.* **115,** 142301
37. Tsigankov, P., Gherardini, P. F., Helmer-Citterich, M., Spath, G. F., Myler, P. J., and Zilberstein, D. (2014) Regulation dynamics of Leishmania differentiation: deconvoluting signals and identifying phosphorylation trends. *Mol. Cell. Proteomics* **13,** 1787–1799
38. Castello, A., Fischer, B., Eichelbaum, K., Horos, R., Beckmann, B. M., Strein, C., Davey, N. E., Humphreys, D. T., Preiss, T., Steinmetz, L. M., Krijgsveld, J., and Hentze, M. W. (2012) Insights into RNA biology from an atlas of mammalian mRNA-binding proteins. *Cell* **149,** 1393–1406
39. Capewell, P., Monk, S., Ivens, A., Macgregor, P., Fenn, K., Walrad, P., Bringaud, F., Smith, T. K., and Matthews, K. R. (2013) Regulation of Trypanosoma brucei total and polysomal mRNA during development within its mammalian host. *PLoS ONE* **8,** e67069
40. Gehring, P., Sowa, J. K., Cremers, J., Wu, Q., Sadeghi, H., Sheng, Y., Warner, J. H., Lambert, C. J., Briggs, G. A. D., and Mol, J. A. (2017) Distinguishing lead and molecule states in graphene-based single-electron transistors. *ACS Nano* **11,** 5325–5331